Elementary excitations in superfluid ^{3}He-^{4}He mixtures

David Mateo and Manuel Barranco
Departament ECM, Facultat de Física, and IN2UB, Universitat de Barcelona, Diagonal 647, 08028 Barcelona, Spain

Jesús Navarro
IFIC, CSIC–University of Valencia, Apartado 22085, 46071 Valencia, Spain

(Received 21 June 2010; revised manuscript received 30 September 2010; published 21 October 2010)

We have studied the dynamic structure function of superfluid ^{3}He-^{4}He mixtures at zero temperature as a function of pressure and ^{3}He concentration. Results obtained in the full random-phase approximation (RPA) plus density-functional theory and in a generalized Landau-Pomeranchuk approach are presented and compared with experiment. Analytic expressions for several sum rules of the dynamic structure functions have been determined, and have been used to obtain average energies of the collective excitations. In the RPA approach, the dispersion relation of the collective modes shows typical features of level repulsion between zero-soundlike and phonon-rotonlike excitations. The structure of the coupled RPA equations for the mixture leads in a natural way to the hybridization of the collective modes. The mixed ^{3}He-^{4}He dynamic structure function quenches the zero-soundlike mode before it crosses the phonon-roton branch, causing that the former mode only appears with enough strength after the crossing.

DOI: 10.1103/PhysRevB.82.134529 PACS number(s): 67.60.−g, 67.90.+z, 31.15.E−

I. INTRODUCTION

Liquid mixtures made of the two stable isotopes of helium, ^{3}He and ^{4}He, have been the subject of a series of experimental and theoretical studies since quite long time ago, and several comprehensive articles have been published covering most aspects of their thermodynamic properties and/or elementary excitation spectrum.[1–10] A distinct property of ^{3}He-^{4}He liquid mixtures is that, at low temperatures, ^{3}He has a limited solubility in ^{4}He,[11] with a maximum ^{3}He concentration (x_3) of about 9.5% at a pressure (P) of $\sim$10 atm. At $P=0$ it is even lower, about 6.5%.

In the dilute regime, these mixtures have been addressed within the Landau-Pomeranchuk (LP) model in which ^{3}He atoms are treated as quasiparticles that do no interact with each other and only feel the interaction with the ^{4}He liquid background. For larger concentrations, ^{3}He-^{3}He interactions were effectively taken into account by nonlocal pseudopotentials, as in the Bardeen *et al.* approach[12] aiming at describing transport properties and the elementary excitation spectrum. Later on, Weyrauch and Szprynger[13] have used a similar approach to work out the density-density response of He mixtures at low temperatures. In Refs. 2 and 3, the density-density response of the mixture was addressed by using a dispersion relation in terms of a frequency matrix of static restoring forces and a complex self-energy matrix. A fully microscopic variational method has allowed to determine the energetics and structure of the ground state of the mixture on one hand, and the elementary excitation spectrum in the random-phase approximation (RPA) on the other hand.[8] Correlated-basis-function perturbation theory has been also used to obtain the response function of ^{3}He-^{4}He liquid mixtures.[14] These works still are the most microscopic evaluation of the static and dynamic properties of liquid-helium mixtures at zero temperature (T). Another variational microscopic approach[15] has been used to determine several relevant energy moments (i.e., sum rules) of the dynamic structure function entering the double-differential cross section for inelastic neutron scattering of liquid-helium mixtures. The evaluation of these sum rules only requires the knowledge of the different pair distribution functions for ^{3}He and ^{4}He atoms in the mixture.

While the thermodynamic properties of helium mixtures have been experimentally studied in detail, information on the pressure and temperature (T) dependence of their elementary excitations is more scarce. It is mainly obtained by neutron scattering experiments difficult to carry out due to the large neutron-absorption cross section of ^{3}He.

A detailed analysis of the neutron-scattering function for dilute mixtures for wave vectors q between 0.4 and 2.2 Å^{-1} was presented by Fåk *et al.*[16] for temperatures in the 0.07–1.5 K range, pressures of 0, 10, and 18 bar, and two values of the ^{3}He concentration, namely, 1% and 5%. They have found that at low T, the excitation spectrum has two branches: a well-defined collective phonon-roton excitation mainly arising from ^{4}He, and a Fermi-gaslike particle-hole (ph) band of ^{3}He origin. The latter result indicates that even for a fairly large ^{3}He concentration of 5%, the ^{3}He-^{3}He interaction is so weak that the mixture cannot sustain a zero-sound-mode excitation. Moreover, the observed area of the ph peak is about 1/3 of that expected for a free-Fermi gas. This is consistent with the absence of a zero-sound mode, as the ^{3}He effective mass m_3^* in the mixture is on the order of $2.4m_3$. In contrast, a zero-sound-modelike excitation was found in the microscopic variational calculations of Ref. 8. It is worth noticing that the experimental analysis of Ref. 16 was carried out neglecting the effect of the mixed ^{3}He-^{4}He dynamic structure function we describe in Sec. II, whose effect in the calculations carried our so far[2,3,8,13,15] and in the present ones has been found to be non-negligible.

In this work, we carry out an analysis of the excitation spectrum of superfluid ^{3}He-^{4}He liquid mixtures within the RPA based on the zero-temperature density-functional (DF) approach of Ref. 17. This approach is the natural extension

to liquid-helium mixtures of those originally proposed for pure ^{4}He and ^{3}He.[18,19] DF methods represent a useful computational tool to study the properties of quantum fluids, providing a good compromise between accuracy and computational cost. As any method based on DF theory, our approach is a phenomenological one that has the virtue of allowing us to address the ground state and excitation spectrum of liquid-helium system, mixed or not, pristine or doped, in a variety of geometries, as bulk liquids, drops,[20] films,[21] and bubbles.[22] We refer the reader to Ref. 23 for a review of the method and of older results on helium droplets. Optimized variational calculations on the dynamics of ^{4}He droplets have been reported in Ref. 24, and DF calculations of the ground state and excitation spectrum of ^{4}He and ^{3}He drops can be found, e.g., in Refs. 18, 25, and 26.

This work is organized as follows. In Sec. II, we describe the density-functional approach we have used to obtain the phase diagram of the superfluid helium mixture at $T=0$, the correlated density-density responses, and their associated dynamic structure functions and sum rules. In Sec. III, we present the results for the total scattering function, and a summary is presented in Sec. IV.

II. DENSITY-FUNCTIONAL APPROACH AT ZERO TEMPERATURE

The particle-hole interaction is a key ingredient to calculate the linear-response function of the system to an external probe. We have derived it from an energy density functional $E[\rho_3,\tau_3,\rho_4]$, described in terms of the particle number densities $\rho_{3,4}$ of each isotope ^{3}He and ^{4}He, respectively, and of the kinetic-energy density τ_3 of ^{3}He. In doing so, we achieve a consistent description of both static and dynamical properties of the liquid mixture.

A. Density functional for superfluid ^{3}He-^{4}He liquid mixtures

Our starting point is the zero-temperature density-functional employed in Ref. 17 to investigate the energetics and structural features of mixed ^{3}He-^{3}He drops. The total energy of a liquid-helium mixture was expressed as a density functional of their particle number densities ρ_4 and ρ_3, and of the kinetic-energy density τ_3 of ^{3}He in the following way:

$$E[\rho_3,\tau_3,\rho_4]=\int d\mathbf{r}\{\mathcal{E}_4[\rho_3,\rho_4]+\mathcal{E}_3[\rho_3,\tau_3,\rho_4]+\mathcal{E}_{34}[\rho_3,\rho_4]\}, \tag{1}$$

where

$$\mathcal{E}_4[\rho_3,\rho_4]=\frac{\hbar^2}{2m_4}(\nabla\sqrt{\rho_4(\mathbf{r})})^2+\frac{1}{2}\int d\mathbf{r}'\rho_4(\mathbf{r})V_4(|\mathbf{r}-\mathbf{r}'|)\rho_4(\mathbf{r}')+\frac{1}{2}c_4'\rho_4(\mathbf{r})[\bar{\rho}_3(\mathbf{r})+\bar{\rho}_4(\mathbf{r})]^2+\frac{1}{3}c_4''\rho_4(\mathbf{r})[\bar{\rho}_3(\mathbf{r})+\bar{\rho}_4(\mathbf{r})]^3$$
$$-\frac{\hbar^2}{4m_4}\alpha_s\int d\mathbf{r}'F(|\mathbf{r}-\mathbf{r}'|)\left[1-\frac{\tilde{\rho}_4(\mathbf{r})}{\rho_{0s}}\right]\nabla\rho_4(\mathbf{r})\cdot\nabla'\rho_4(\mathbf{r}')\left[1-\frac{\tilde{\rho}_4(\mathbf{r}')}{\rho_{0s}}\right], \tag{2}$$

$$\mathcal{E}_3[\rho_3,\tau_3,\rho_4]=\frac{\hbar^2}{2m_3^*}\tau_3(\mathbf{r})+\frac{1}{2}\int d\mathbf{r}'\rho_3(\mathbf{r})V_3(|\mathbf{r}-\mathbf{r}'|)\rho_3(\mathbf{r}')$$
$$+\frac{1}{2}c_3'\rho_3^2(\mathbf{r})[\bar{\rho}_3(\mathbf{r})+\bar{\rho}_4(\mathbf{r})]^{\gamma_3}+\frac{1}{2}c_3''\rho_3^2(\mathbf{r})\bar{\rho}_3^{\gamma_3}(\mathbf{r}), \tag{3}$$

and

$$\mathcal{E}_{34}[\rho_3,\rho_4]=\int d\mathbf{r}'\rho_3(\mathbf{r})V_{34}(|\mathbf{r}-\mathbf{r}'|)\rho_4(\mathbf{r}')$$
$$+c_{34}\rho_3(\mathbf{r})\rho_4(\mathbf{r})[\bar{\rho}_3(\mathbf{r})+\bar{\rho}_4(\mathbf{r})]^{\gamma_{34}}. \tag{4}$$

In these expressions, $\bar{\rho}_i$ for $i=3,4$ are averaged densities given by

$$\bar{\rho}_i(\mathbf{r})=\int d\mathbf{r}'\rho_i(\mathbf{r}')w_i(|\mathbf{r}-\mathbf{r}'|), \tag{5}$$

where

$$w_i(r)=\frac{3}{4\pi h_i^3}\quad \text{if } r<h_i$$
$$=0\quad \text{otherwise}. \tag{6}$$

In addition V_i ($i=3$, 4, or 34) is a finite range interaction consisting of a Lennard-Jones (LJ) potential with truncated core

$$V_i(r)=4\epsilon_{LJ}\left[\left(\frac{\sigma_i}{r}\right)^{12}-\left(\frac{\sigma_i}{r}\right)^{6}\right]\quad \text{if } r>h_i$$
$$=0\quad \text{otherwise}. \tag{7}$$

A Gaussian kernel

$$F(r)=\frac{1}{\pi^{3/2}l^3}e^{-r^2/l^2} \tag{8}$$

with dispersion $l=1$ Å is used to define the other averaged density entering $\mathcal{E}_4$,

$$\tilde{\rho}_4(\mathbf{r}) = \int d\mathbf{r}' \rho_4(\mathbf{r}') F(|\mathbf{r}-\mathbf{r}'|). \tag{9}$$

$\mathcal{E}_4$ reduces to the Orsay-Trento (OT) density functional[18] setting ρ_3 to zero. $\mathcal{E}_3$ and $\mathcal{E}_{34}$ are finite-range generalizations of the density functional introduced in Ref. 27, with an effective mass of ^{3}He parametrized so as to fit the experimental data of Ref. 28,

$$\frac{\hbar^2}{2m_3^*} = \frac{\hbar^2}{2m_3}\left(1 - \frac{\bar{\rho}_3}{\rho_{3c}} - \frac{\bar{\rho}_4}{\rho_{4c}}\right)^2. \tag{10}$$

In this paper, we have modified the kinetic-energy contribution so as to preserve translational invariance, along the same lines as in Ref. 26, which amounts to replace the kinetic-energy density τ_3 entering $\mathcal{E}_3$ with $\tau_3 - \mathbf{j}_3^2/\rho_3$, where $\mathbf{j}_3$ is the current density of ^{3}He. For systems having an effective mass m^*, this modification is required to guarantee that the density functional is Galilean invariant.[29] This term has no influence on the ground state of time-reversal invariant, spin-saturated droplets, and for this reason it is usually omitted.[17] However, its contribution to the ph interaction must be taken into account.

In a similar spirit, a current-current term was considered in Ref. 18 to reproduce dynamical properties of ^{4}He systems, based on the OT density functional. Such a contribution acts as a backflow term, to which a q-dependent ^{4}He effective mass is associated as

$$\frac{\hbar^2}{2m_4^*(q)} = \frac{\hbar^2}{2m_4}\{1 - \rho_4[\hat{V}_J(0) - \hat{V}_J(q)]\}, \tag{11}$$

where $\hat{V}_J(q)$ is the Fourier transform of the effective current-current interaction, fitted so as to reproduce the maxon-roton dispersion curve in liquid ^{4}He.[18] Setting either ρ_3 or ρ_4 equal to zero, the functional reproduces also ground-state properties of ^{4}He or ^{3}He liquids, respectively. The set of coefficients of the whole density functional is taken from Ref. 17. However, the screened Lennard-Jones parameter h_3 entering the definition of the coarse-grained ^{3}He density $\bar{\rho}_3$ has been multiplied by a factor 1.8 as proposed in Ref. 30.

Altogether, this density functional allows for an accurate description of thermodynamical properties of the mixed liquid, such as the maximum solubility of ^{3}He into liquid ^{4}He, the excess volume coefficient and the osmotic pressure at various pressures between 0 and 20 atm for the liquid mixture. This is at variance with the polarization potentials approach, whose main concern was to describe transport properties in dilute solutions of ^{3}He in ^{4}He.[7] We also want to mention that the full microscopic approach, despite its high overall precision,[8] only yields a qualitative agreement for the maximum solubility of ^{3}He in ^{4}He, indicating that this is a subtle property of the mixture whose description still seems beyond current microscopic approaches.

Figure 1 represents the zero-temperature phase diagram of the ^{3}He-^{4}He mixture determined within our DF approach. We show the ^{3}He maximum concentration line—or ^{3}He segregation line—obtained at $T=0$ by solving the two-phase equilibrium conditions

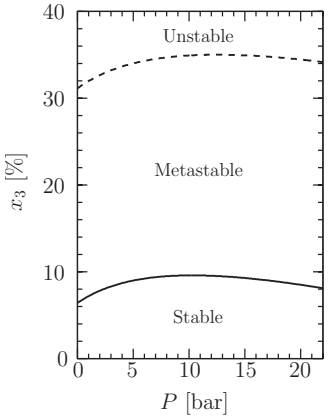

FIG. 1. Phase diagram of the ^{3}He-^{4}He liquid mixture at $T=0$ K. The solid line represents the ^{3}He segregation line and the dashed line the spinodal line.

$$P(\rho, x_3) = P(\rho_3, x_3 = 1),$$

$$\mu_3(\rho, x_3) = \mu_3(\rho_3, x_3 = 1) \quad , \tag{12}$$

where μ_3 is the ^{3}He chemical potential, $\rho = \rho_3 + \rho_4$ is the total liquid density, and $x_3 = \rho_3/(\rho_4 + \rho_3)$ is the ^{3}He concentration. Also displayed is the spinodal line that separates the metastable and unstable regions in the phase diagram. We recall that necessary and sufficient stability conditions for a binary mixture at $T=0$ are

$$\mathcal{K} = \left(\frac{\partial P}{\partial \rho}\right)_{x_3} \geq 0,$$

$$\left(\frac{\partial \mu_4}{\partial x_3}\right)_P \leq 0 \quad \text{or} \quad \left(\frac{\partial \mu_3}{\partial x_3}\right)_P \geq 0, \tag{13}$$

where $\mathcal{K}$ is the compressibility of the liquid. In the present case, it is the second of the above conditions that is violated first and thus defines the spinodal line. For larger ^{3}He concentrations, the homogeneous mixture is thermodynamically unstable. Note that the metastability region between the ^{3}He segregation and spinodal lines is fairly wide.

B. Particle-hole interactions

The particle-hole interactions are defined as functional derivatives of the total energy in the following way:

$$V_{ph}^{(\alpha,\beta)} = \frac{\delta^2 E[\rho_3, \tau_3, \rho_4]}{\delta \rho^{(\alpha)}_{\mathbf{k}_3,\mathbf{k}_1} \delta \rho^{(\beta)}_{\mathbf{k}_4,\mathbf{k}_2}}, \tag{14}$$

where $\rho_{i,j}^{(\alpha)}$ are density occupation numbers, the indices α, β take the values 3,4 corresponding to each isotope, and $(\mathbf{k}_3, \mathbf{k}_1)$ and $(\mathbf{k}_4, \mathbf{k}_2)$ refer to the momenta of the particle-hole pairs 1,3 and 2,4, respectively. Because of momentum conservation, there are actually three independent momenta. We choose them as the external momentum transfer $\mathbf{q}$, and the momenta $\mathbf{k}$ and $\mathbf{k}'$ of the initial and final holes: $\mathbf{k}_1 = \mathbf{q} + \mathbf{k}$, $\mathbf{k}_2 = \mathbf{k}'$, $\mathbf{k}_3 = \mathbf{k}$, and $\mathbf{k}_4 = \mathbf{q} + \mathbf{k}'$, following the same notation as Ref. 30. A clear advantage of using a density functional is

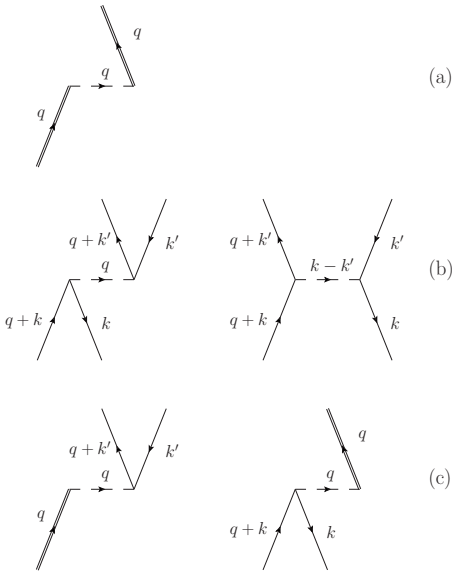

FIG. 2. Particle-hole interactions: (a) 4-4, (b) 3-3, direct and exchange terms, (c) 4-3 and 3-4.

that it is defined in the whole range of densities and concentrations for which the liquid-helium mixture is at least metastable, and therefore so are the particle-hole interactions and response functions defined in the next subsection, and no further ingredients are needed to obtain the elementary excitations.

As for the ^{4}He, there are no holes because at $T=0$ all bosons are in the condensate. There is just a single excitation for a given external momentum $\mathbf{q}$, whose energy is $\hbar^2q^2/2m_4^*$. The ph interaction is depicted diagrammatically in Fig. 2(a). There are two contributions to the (3,3) particle-hole interaction, as represented in Fig. 2(b). The first diagram corresponds to the Hartree contribution, and the second one takes into account the exchange between fermions. The particle-hole interaction for fermions is thus properly antisymmetrized. Finally, there are two mixed particle-hole interactions, as a ^{4}He excitation can generate a ^{3}He particle-hole pair or vice versa. These two interactions are depicted in Fig. 2(c).

Taking into account these considerations, and with the notation of Fig. 2, the functional derivative of the density functional yields the following particle-hole interactions. For the ^{4}He-^{4}He component,

$$V_{ph}^{(4,4)} = \hat{V}_4(q) + c_4'\{2\rho\hat{w}_4(q) + \rho_4\hat{w}_4^2(q)\} + 2c_4''\{\rho^2\hat{w}_4(q) + \rho_4\rho\hat{w}_4^2(q)\} - \frac{\hbar^2}{2m_4}\alpha_s\left(1 - \frac{\rho_4}{\rho_{0s}}\right)^2 q^2 e^{-(ql)^2/4} + \frac{\hbar^2}{2m_3}\frac{2}{\rho_{4c}^2}\hat{w}_4^2(q)\tau_3 + c_3'\frac{1}{2}\gamma_3(\gamma_3-1)\rho_3^2\rho^{\gamma_3-2}\hat{w}_4^2(q) + c_{34}\gamma_{34}\rho^{\gamma_{34}-2}[2\rho_3\rho\hat{w}_4(q) + \rho_3\rho_4(\gamma_{34}-1)\hat{w}_4^2(q)] + \frac{\hbar^2q^2}{4m_4}[\hat{V}_J(0) - \hat{V}_J(q)], \tag{15}$$

where $\hat{V}_\alpha(q)$ and $\hat{\omega}_\alpha(q)$ are the Fourier transform of the screened Lennard-Jones potentials and $\omega_\alpha(r)$ functions, respectively. In view of the low ^{3}He concentrations, for the ^{3}He-^{3}He component we only consider the spin-symmetric channel, and restrict ourselves to the case were the fermionic holes are created at the Fermi surface ($k=k_F, k'=k_F$), considering only the monopolar and dipolar parts ($\mathbf{q}\cdot\mathbf{k}=0, \mathbf{q}\cdot\mathbf{k}'=0, \mathbf{k}\cdot\mathbf{k}'=k_F^2\cos\theta\cos\theta'$) of the ph interaction,

$$\begin{aligned} 2V_{ph}^{(3,3)} &= \hat{V}_3(q) + c_3'\rho^{\gamma_3-2}\left[\rho^2 + 2\rho_3\rho\gamma_3\hat{w}_3(q) + \frac{1}{2}\gamma_3(\gamma_3-1)\rho_3^2\hat{w}_3^2(q)\right] + c_3''\rho^{\gamma_3}\left[1 + 2\gamma_3\hat{w}_3(q) + \frac{1}{2}\gamma_3(\gamma_3-1)\hat{w}_3^2(q)\right] + c_4'\rho_4\hat{w}_3^2(q) + 2c_4''\rho_4\rho\hat{w}_3^2(q) \\ &+ c_{34}\gamma_{34}\rho^{\gamma_{34}-2}[2\rho_4\rho\hat{w}_3(q) + \rho_3\rho_4(\gamma_{34}-1)\hat{w}_3^2(q)] + \frac{\hbar^2}{2m_3}\frac{2}{\rho_{3c}^2}\hat{w}_3^2(q)\tau_3 - \frac{\hbar^2}{2m_3}\left(1 - \frac{\rho_3}{\rho_{3c}} - \frac{\rho_4}{\rho_{4c}}\right)\frac{2}{\rho_{3c}}\hat{w}_3(q)2k_F^2 + \frac{2}{\rho_3}\left(\frac{\hbar^2k_F^2}{2m_3} - \frac{\hbar^2k_F^2}{2m_3^*}\right)\cos\theta\cos\theta' \\ &\equiv f_0(q) + f_1\cos\theta\cos\theta'. \end{aligned} \tag{16}$$

The prefactor of 2 takes into account the spin degeneracy. We have decomposed this interaction in its Landau fields $f_0(q)$ and f_1. This expression contains the two contributions depicted in Fig. 2(b), and it is completely antisymmetric. Consistent with the Landau-type approximation we are using, the mixed components are

$$\begin{aligned} V_{ph}^{(4,3)} &= \hat{V}_{34}(q) + c_{34}\rho^{\gamma_{34}-2}\{\rho^2 + \gamma_{34}\rho_4\rho\hat{w}_4(q) + \gamma_{34}\rho_3\rho\hat{w}_3(q) + \gamma_{34}(\gamma_{34}-1)\rho_3\rho_4\hat{w}_3(q)\hat{w}_4(q)\} + c_3'\rho^{\gamma_3-2}\left[\gamma_3\rho_3\rho\hat{w}_4(q) + \frac{1}{2}\gamma_3(\gamma_3-1)\rho_3^2\hat{w}_3(q)\hat{w}_4(q)\right] + c_4'[\rho\hat{w}_3(q) \\ &+ \rho_4\hat{w}_3(q)\hat{w}_4(q)] + c_4''[\rho^2\hat{w}_3(q) + 2\rho_4\rho\hat{w}_3(q)\hat{w}_4(q)] + \frac{\hbar^2}{2m_3}\frac{2}{\rho_{3c}\rho_{4c}}\hat{w}_3(q)\hat{w}_4(q)\tau_3 - \frac{\hbar^2}{2m_3}\left(1 - \frac{\rho_3}{\rho_{3c}} - \frac{\rho_4}{\rho_{4c}}\right)\frac{2}{\rho_{4c}}\hat{w}_4(q)k_F^2 \end{aligned} \tag{17}$$

with $V_{ph}^{(3,4)} = V_{ph}^{(4,3)}$.

In Fig. 3, the resulting ph interactions are depicted as a function of the transferred momentum q. They are compared with the polarization potentials of Pines and collaborators,[7,31,32] with which they bear some analogies, and with the ph interactions calculated by Krotscheck and Saarela[8] by means of an optimized microscopic calculation based on the hypernetted chain theory. From Fig. 3, we can see that the three approaches provide qualitatively similar ph

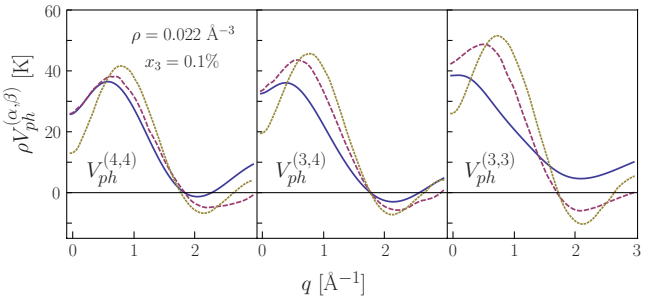

FIG. 3. (Color online) Particle-hole interactions calculated for a ^{3}He concentration x_3=0.1% and a total density ρ=0.022 Å^{-3}. Solid lines: this work; dashed lines: Ref. 7; dotted lines: Ref. 8. For the sake of comparison, the ph interactions have been multiplied by the total helium density ρ. In the right panel, the solid line actually corresponds to the f_0 interaction as defined in Eq. (16).

interactions. Since they are subsequently used within different many-body schemes, it is difficult to ascertain the physical relevance of their apparent differences.

C. Response functions

We consider now the response function of the mixed system to density fluctuations. There are two density operators

$$\rho_{\mathbf{q}}^{(\alpha)} = \sum_{j=1}^{N_\alpha} e^{i\mathbf{q}\cdot\mathbf{r}_j}, \tag{18}$$

where N_α is the number of particles of α type, either 3 or 4, and four response functions $\chi^{(\alpha,\beta)}$, which are defined as

$$\chi^{(\alpha,\beta)}(q,\omega) = \sum_n \left[\frac{\langle 0|\rho_{\mathbf{q}}^{(\alpha)\dagger}|n\rangle\langle n|\rho_{\mathbf{q}}^{(\beta)}|0\rangle}{\omega - \omega_{n0} + i\eta} - \frac{\langle 0|\rho_{\mathbf{q}}^{(\beta)\dagger}|n\rangle\langle n|\rho_{\mathbf{q}}^{(\alpha)}|0\rangle}{\omega + \omega_{n0} + i\eta} \right], \tag{19}$$

where $|0\rangle$ and $|n\rangle$ stand for the ground and excited many-body state, respectively, and $\hbar\omega_{n0}=E_n-E_0$ is the excitation energy of state $|n\rangle$. The noninteracting response functions are diagonal in α and β. Their expressions at T=0 are given in standard many-body textbooks, see, e.g., Ref. 33. In our case, all bosons are in the condensate and there is no hole propagator,

$$\chi_0^{(4)}(q,\omega) = \frac{\dfrac{\hbar^2 q^2}{m_4^*}\rho_4}{\hbar^2(\omega+i\eta)^2 - \left(\dfrac{\hbar^2 q^2}{2m_4^*}\right)^2}. \tag{20}$$

For fermions, using the following dimensionless variables:

$$k = \frac{q}{2k_F}, \quad \nu = \frac{(\omega+i\eta)m_3^*}{\hbar q k_F}, \tag{21}$$

one gets

$$\chi_0^{(3)}(q,\omega) = -\frac{m_3^* k_F}{\hbar^2 2\pi^2}\left\{1 + \frac{1}{4k}[1-(k+\nu)^2]\log\left(\frac{k+\nu+1}{k+\nu-1}\right) + \frac{1}{4k}[1-(k-\nu)^2]\log\left(\frac{k-\nu+1}{k-\nu-1}\right)\right\}. \tag{22}$$

Unless explicited otherwise, the results presented in the following figures have been obtained with a small but finite value for η, namely, $\hbar\eta$=0.1 K.

The ph interactions couple the response functions $\chi^{(\alpha,\beta)}$, and in general it is not an easy task to obtain explicit expressions for them because $V_{ph}^{(\alpha,\beta)}$ depend on the fermionic hole momenta. Let us assume for the moment that the ph interactions only depend on the transferred momentum q. We shall employ the simplified notation

$$W_4(q) = V_{ph}^{(4,4)}, \quad W_x(q) = V_{ph}^{(4,3)} = V_{ph}^{(3,4)}, \quad W_3(q) = V_{ph}^{(3,3)} \tag{23}$$

for the ph interactions, and analogously for the response functions $\chi^{(\alpha,\beta)}(q,\omega)$ and the dynamic structure functions

$$S^{(\alpha,\beta)}(q,\omega) = -\frac{1}{\pi}\mathrm{Im}\,\chi^{(\alpha,\beta)}(q,\omega). \tag{24}$$

In this case, the RPA equations reduce to an algebraic system of coupled equations

$$\chi^{(\alpha,\beta)}(q,\omega) = \chi_0^{(\alpha)}(q,\omega)\delta_{\alpha,\beta} + \chi_0^{(\alpha)}(q,\omega)\sum_\gamma V_{ph}^{(\alpha,\gamma)}(q)\chi^{(\gamma,\beta)}(q,\omega), \tag{25}$$

whose solution is straightforward. To help understanding the hybridization of the ^{4}He and ^{3}He modes, we shall discuss later on, we write the solutions in the following way:

$$\chi^{(4)}(q,\omega) = \frac{\chi_{uc}^{(4)}(q,\omega)}{1 - \frac{1}{2}[W_x(q)]^2\chi_{uc}^{(3)}(q,\omega)\chi_{uc}^{(4)}(q,\omega)},$$

$$\chi^{(3)}(q,\omega) = \frac{\chi_{uc}^{(3)}(q,\omega)}{1 - \frac{1}{2}[W_x(q)]^2\chi_{uc}^{(3)}(q,\omega)\chi_{uc}^{(4)}(q,\omega)},$$

$$\chi^{(x)}(q,\omega) = \frac{W_x(q)\chi_{uc}^{(4)}(q,\omega)\chi_{uc}^{(3)}(q,\omega)}{1 - \frac{1}{2}[W_x(q)]^2\chi_{uc}^{(3)}(q,\omega)\chi_{uc}^{(4)}(q,\omega)}. \tag{26}$$

In these expressions, we have introduced the "uncoupled" responses

$$\chi_{uc}^{(4)}(q,\omega) = \frac{\chi_0^{(4)}(q,\omega)}{1 - W_4(q)\chi_0^{(4)}(q,\omega)},$$

$$\chi_{uc}^{(3)}(q,\omega) = \frac{\chi_0^{(3)}(q,\omega)}{1 - W_3(q)\chi_0^{(3)}(q,\omega)}. \tag{27}$$

Formally, these response functions have the same structure as for the pure systems, with the important difference that the ph interactions W_α include the effect of both isotopes. Ex-

pressions similar to Eq. (26) have been introduced in Ref. 13. This shows that our RPA-DF method bears some similarities with the polarization potential method used in that reference, with the key difference that in our approach, the particle-hole interaction is obtained by functional derivative of a density functional that also yields the ground-state properties of the mixture in bulk liquid and in finite configurations (drops and films) as well.[23]

In the Appendix, we show that the same structure is maintained in the Landau approximation of Eq. (16). The only modification is that the interaction W_3 depends also on the transferred energy ω in the following way:

$$W_3(q,\omega) = f_0(q) + \frac{f_1 \nu^2}{1 + F_1/3}, \tag{28}$$

where F_1 is the dimensionless Landau parameter obtained multiplying f_1 with the level density $N_0 = k_F m_3^*/(\hbar^2 \pi^2)$.

Equations (26) show that the pole structure of all these responses is the same. This means that, on one hand, some hybridization of the ^{3}He (^{4}He) modes is expected because of the presence of the ^{4}He (^{3}He) component and, on the other hand, the mixed $\chi^{(x)}$ response does not contain any collective state not present already in $\chi^{(3)}$ and $\chi^{(4)}$.

D. Sum rules

Sum rules are often used to characterize global properties of the response functions. For general properties of sum rules, we address the reader to Refs. 34 and 35. The nth sum rule is defined as

$$M_n^{(\alpha,\beta)}(q)/N = \frac{1}{\rho}\int d(\hbar\omega)(\hbar\omega)^n S^{(\alpha,\beta)}(q,\omega). \tag{29}$$

We use for the sum rules the same simplified notation as for the ph interactions and the response functions.

Sum rules M_1 (also called f-sum rule) and M_3 can be obtained as the ground-state expectation value of nested commutators of the Hamiltonian and the density operator, as done by Boronat *et al.* for the mixed ^{3}He-^{4}He system.[15] Alternatively, these two sum rules can also be obtained from the first two coefficients, $1/\omega^2$ and $1/\omega^4$, in a $\omega \to \infty$ expansion of the response functions. From Eq. (26) we obtain

$$M_1^{(4)}/N = (1 - x_3)\frac{\hbar^2 q^2}{2m_4^*},$$

$$M_1^{(3)}/N = x_3 \frac{\hbar^2 q^2}{2m_3},$$

$$M_1^{(x)}/N = 0,$$

$$M_3^{(4)}/N = \frac{1}{2}(1 - x_3)\left(\frac{\hbar^2 q^2}{m_4^*}\right)^2 \left\{\frac{\hbar^2 q^2}{4m_4^*} + \rho_4 W_4\right\},$$

$$M_3^{(3)}/N = \frac{1}{2}x_3\left(\frac{\hbar^2 q^2}{m_3}\right)^2 \left\{\rho_3 f_0 + \frac{\hbar^2 k_F^2}{m_3^*}\left(\frac{3}{5} + \frac{q^2}{4k_F^2}\right)\right\},$$

$$M_3^{(x)}/N = \frac{1}{2}\frac{\hbar^2 q^2}{m_3}\frac{\hbar^2 q^2}{m_4^*} W_x \sqrt{\rho_4 \rho_3}. \tag{30}$$

The inverse energy-weighted sum rule M_{-1} is proportional to the response function at zero frequency. From Eq. (26) again, we obtain

$$M_{-1}^{(4)}/N = (1 - x_3)\left\{\frac{\hbar^2 q^2}{2m_4^*} + 2W_4\rho_4 - \frac{W_x^2 \rho_4 \rho_3 f(k)}{\frac{\hbar^2 k_F^2}{3m_3^*} + f_0 \rho_3 f(k)}\right\}^{-1},$$

$$M_{-1}^{(3)}/N = x_3 \frac{f(k)}{2}\left\{\frac{\hbar^2 k_F^2}{3m_3^*} + f_0\rho_3 f(k) - \frac{W_x^2 \rho_4 \rho_3 f(k)}{\frac{\hbar^2 q^2}{2m_4^*} + 2W_4\rho_4}\right\}^{-1},$$

$$M_{-1}^{(x)}/N = \sqrt{x_3(1 - x_3)} f(k)\left\{W_x\sqrt{\rho_4\rho_3} f(k) - \frac{\left(\frac{\hbar^2 q^2}{2m_4^*} + 2\rho_4 W_4\right)\left[\frac{\hbar^2 k_F^2}{3m_3^*} + f_0\rho_3 f(k)\right]}{W_x\sqrt{\rho_4\rho_3}}\right\}^{-1}, \tag{31}$$

where we have defined

$$f(k) = \frac{1}{2}\left[1 + \frac{1}{2k}(1 - k^2)\log\left|\frac{k+1}{k-1}\right|\right] \tag{32}$$

with $k = q/(2k_F)$.

There is no close expression for the nonenergy-weighted sum rule $M_0^{(\alpha)}$, which can be obtained by direct integration of Eq. (29). $M_0^{(\alpha)}$ is nothing but the static structure factor $S^{(\alpha)}(q)$, which is related to the two-body density distribution and for this reason cannot be addressed within the DF approach. However, we have checked that the $M_0^{(\alpha)}$ moments obtained in our approach bear a structure similar to the microscopic ones.[15] In particular, $M_0^{(x)}(q)$ oscillates as a function of q, being negative, e.g., for $q \lesssim 1.8$ Å^{-1}.

In contrast, as seen in Eqs. (30) and (31), odd-order sum rules are expressed in terms of one-body densities plus ph interaction terms, and are thus naturally adapted to a DF description. The ratio of energy-weighted and nonenergy-weighted sum rules $M_1^{(\alpha)}/M_0^{(\alpha)}$ is the so-called Feynmann dispersion relation,[36] and it is often used in the microscopic calculations to analyze the excitation spectrum.[8,14,15]

The expressions of $M_1^{(\alpha)}$, $M_3^{(\alpha)}$, and $M_{-1}^{(\alpha)}$ for $\alpha = 3, 4$ can be used to obtain two average excitation energies, namely,[34,35]

$$\hbar\omega_3^{(\alpha)} = \sqrt{M_3^{(\alpha)}/M_1^{(\alpha)}} \quad \text{and} \quad \hbar\omega_1^{(\alpha)} = \sqrt{M_1^{(\alpha)}/M_{-1}^{(\alpha)}}. \tag{33}$$

General properties of sum rules allow one to establish the following inequalities:[34]

$$\hbar\omega_1 \le \frac{M_1^{(\alpha)}}{M_0^{(\alpha)}} \le \hbar\omega_3. \tag{34}$$

The calculated average energies $\hbar\omega_1^{(\alpha)}$ and $\hbar\omega_3^{(\alpha)}$ are depicted in Fig. 4 as a function of q for $P = 0$ and $x_3 = 5\%$, together

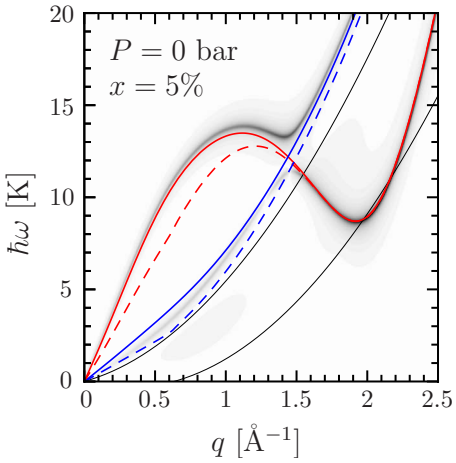

FIG. 4. (Color online) Average energies $\hbar\omega_3$ (solid lines) and $\hbar\omega_1$ (dashed lines) from $S^{(4)}$ and $S^{(3)}$ at $P=0$ bar and $x_3=5\%$. The gray spots are the total scattering function $\hat{S}$ for the mixture at the same conditions. The darker the gray, the larger the value of the scattering function. Also shown is the ph band limited by thin solid lines.

with the ph band, whose limits are defined as[37]

$$0 \le \hbar\omega_{ph} \le \frac{\hbar^2 q^2}{2m_3^*} + \frac{\hbar^2 q k_F}{m_3^*} \quad \text{for } q \le 2k_F,$$

$$\frac{\hbar^2 q^2}{2m_3^*} - \frac{\hbar^2 q k_F}{m_3^*} \le \hbar\omega_{ph} \le \frac{\hbar^2 q^2}{2m_3^*} + \frac{\hbar^2 q k_F}{m_3^*} \quad \text{for } q \ge 2k_F. \tag{35}$$

III. TOTAL SCATTERING FUNCTION

Following Fåk *et al.*[16] (see also Ref. 38), we have defined the total scattering function $\hat{S}(q,\omega)$ as

$$\hat{S}(q,\omega) \equiv \frac{\sigma_4^c S^{(4)}(q,\omega) + (\sigma_3^c + \sigma_3^j) S^{(3)}(q,\omega) + \sigma_{34}^c S^{(x)}(q,\omega)}{\sigma_4^c (1-x_3) + (\sigma_3^c + \sigma_3^j) x_3}, \tag{36}$$

where the elementary cross sections in units of barns are $\sigma_4^c=1.34$, $\sigma_3^c=4.42$, $\sigma_3^j=1.19$, and $\sigma_{34}^c=4.70$. The differences between our expression and that of Ref. 16 arise from the different definition and normalization of the structure functions. In spite of this, both expressions are equivalent. In view of the weak ^{3}He-^{3}He interaction due to the smallness of x_3, we have assumed that the coherent and incoherent dynamic structure functions for ^{3}He are the same.[15,16] $\hat{S}(q,\omega)$ is proportional to the double-differential cross section for inelastic neutron scattering, and displays peaks whose dispersion relation $\omega(q)$ is roughly associated with either ^{3}He or ^{4}He elementary excitations.

Figures 4 and 5 represent $\hat{S}(q,\omega)$ in the full RPA-DF approach for $P=0$, $x_3=5\%$, and for $P=10$ bars and $x_3=1\%$, 5%, 7%, and 9%, respectively. We have chosen the latter P value to have a thermodynamically stable ^{3}He-^{4}He mixture with a large x_3 value, see Fig. 1.

Figure 5 shows that the total scattering function is made of a phonon-rotonlike branch, and of a faint zero-soundlike branch that, at low-q values, appears above the ph band—see Fig. 4. The strength of this zero-soundlike structure increases after it intersects the phonon-roton branch. Actually, the crossing is hindered by a conspicuous level repulsion around $q \sim 1.5$ Å^{-1}. A similar effect was found in Ref. 8. The repulsion gap increases as x_3 does, and the q value at which the level repulsion appears is rather insensitive to the ^{3}He concentration. Indeed, we have found that the phonon-maxon part of the pure ^{4}He dispersion relation is very little affected when we add to it a $x_3=5\%$ ^{3}He while the roton minimum is displaced upward by about 5%.

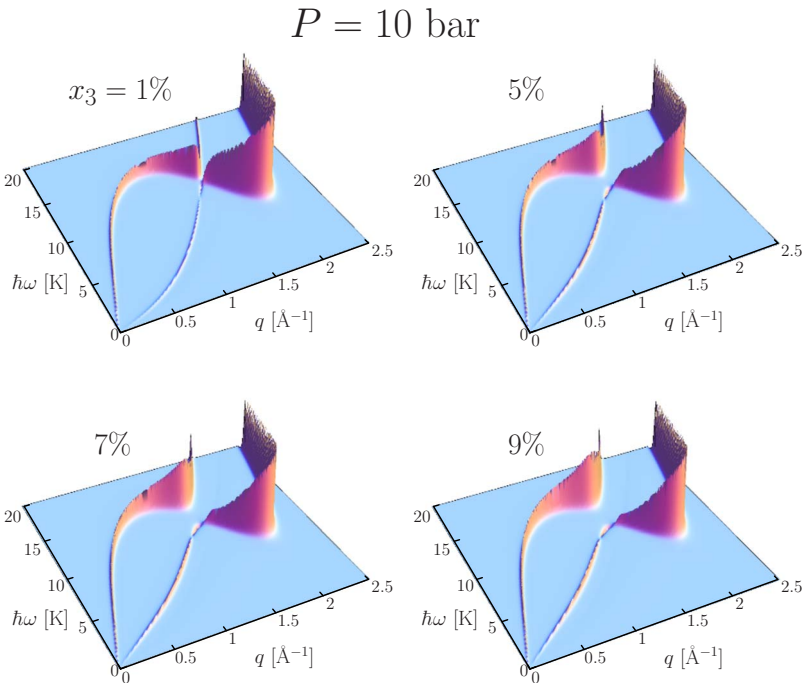

FIG. 5. (Color online) Total scattering function $\hat{S}$ for $P=10$ bars and ^{3}He concentrations x_3 =1%, 5%, 7%, and 9%.

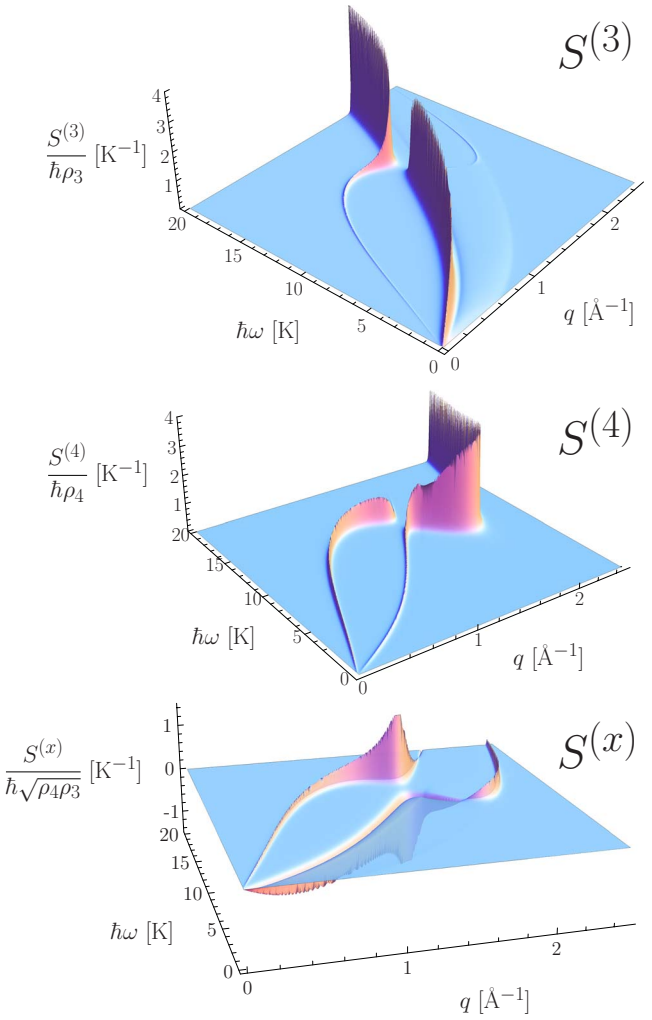

FIG. 6. (Color online) Dynamic structure functions $S^{(3)}$ (top panel), $S^{(4)}$ (middle panel), and $S^{(x)}$ (bottom panel) for $P=0$ bar and $x_3=5\%$. In the top panel, a weak ph band can be seen for energies slightly below the collective mode. The panels have been drawn from different perspectives to help visualize the effects discussed in the text.

To analyze the effect of $S^{(x)}$, i.e., of W_x on $\hat{S}$ and determine to what extent the collective modes are hybridized, we have plotted in Fig. 6 the dynamic structure functions $S^{(4)}/(\hbar\rho_4)$, $S^{(3)}/(\hbar\rho_3)$, and $S^{(x)}/(\hbar\sqrt{\rho_4\rho_3})$ for the same conditions as in Fig. 4. As anticipated, their aspect is similar: all three are significantly nonzero for the same (q,ω) values, although the intensity of each function is different. Moreover, it can be seen that $S^{(x)}$ is negative along the lower energy branch up to nearly the roton minimum, mostly affecting the ^{3}He collective excitation and producing a strong cancellation of the zero-soundlike mode before the crossing while strengthening it after the crossing. This cancellation also appeared in the sum-rule analysis carried out by Boronat *et al.*, see also Refs. 2, 3, 8, and 13. Figure 6 shows that neither the phonon-roton branch nor the zero-sound branch are made of pure—or nearly pure—^{4}He or ^{3}He excitations: both modes are hybridized due to their coupling by the W_x ph interaction. This was also one of the main conclusions of Ref. 13.

Since at $T=0$ K, the mixture can be in a metastable state for ^{3}He concentrations up to $x_3 \gtrsim 30\%$, as shown in Fig. 1, it may be interesting to see the appearance of the total scattering functions for larger x_3 values. One should be aware, however, that reaching a high metastability is very unlikely. It is worth mentioning that, at very low temperatures, metastable ^{3}He-^{4}He solutions have been experimentally found only up to a minute $\Delta x_3=0.3\%$ above the saturation value.[39] In Fig. 7, we display $\hat{S}$ for $P=0$ and $x_3=1\%$, 10%, 20%, and 30%. It is somewhat surprising that the zero-soundlike mode is still quenched even at so large ^{3}He concentrations. Quite naturally, we have found that the larger the x_3, the higher the degree of hybridization of the collective modes.

The analysis of the experimental results carried out in Ref. 16 assumed that $S^{(x)}$ is small and can be neglected. This would imply that energy peaks in $\hat{S}$ can be associated with either ^{3}He excitations, there identified with the particle-hole band, or with the phonon-roton ^{4}He excitations. These authors recognize that their assumption is not obvious, but point out that there is no direct evidence of this crossing term in $\hat{S}$. Our calculations, as Fig. 6 indicates, show the impossibility of disentangling "pure" ^{3}He from ^{4}He excitations. A clear signature of a $S^{(x)}$ effect would be the level repulsion found here and in other microscopic RPA calculations.[8] However, the level repulsion seems not to show up in the experiment.

Experimentally,[16] the total scattering function is dominated by a phonon-roton branch. Rather than a zero-sound branch, a particle-hole band structure appears at low-q, as shown in the top left panel of Fig. 8 taken from that reference. As discussed there, the q dispersion of this branch and the value of the f-sum rule it takes are compatible with the result one would obtain using the "free" fermion expression for the response function, Eq. (22), instead of the RPA one. The limits of the free-Fermion response are those indicated by Eq. (35) using Eq. (10) for m_3^*. This would mean that, due to the low ^{3}He concentration, the weak ^{3}He-^{3}He interaction cannot produce collective modes of zero-sound type in the mixture.

Motivated by these findings, we have switched off the $V_{ph}^{(3,3)}$ interaction, and have redone some calculations keeping all other ^{4}He-^{4}He and ^{3}He-^{4}He contributions, as they are not small. This approximation goes beyond the Landau-Pomeranchuk (LP) approach,[40] that just keeps the quadratic-q quasiparticle spectrum with the effective mass Eq. (10). The LP approximation amounts to setting $W_x=0$ too, in which case the ^{3}He and ^{4}He responses are uncoupled and the dynamic structure function is just the sum of those corresponding to either isotope. Both helium populations would be correlated only throughout the equation of state of the liquid—which is also supplied by the DF approach in this approximation—that gives the total density once the pressure and composition are fixed. We shall refer to the approach in which just $V_{ph}^{(3,3)}$ is set to zero as the generalized LP (GLP) approach. In this approach, the ^{3}He contribution is not merely the ph band but the result of solving the RPA equations with the nonzero W_x contribution.

In Fig. 8, the experimental results of Ref. 16 at saturation vapor pressure (SVP) for $T=70$ mK and $x_3=5\%$ are com-

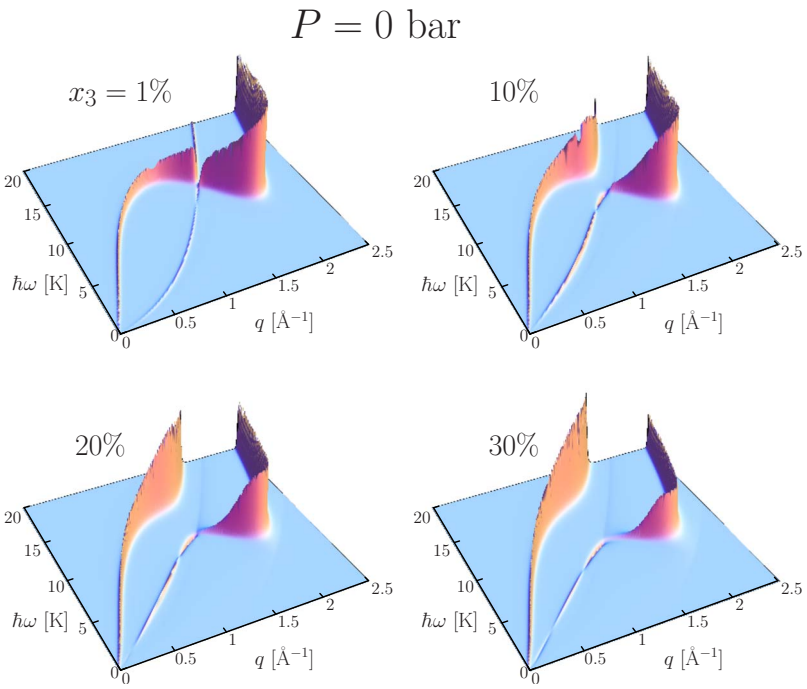

FIG. 7. (Color online) Total scattering function $\hat{S}$ for $P=0$ bar and ^{3}He concentrations $x_3=1\%$, 10%, 20%, and 30%.

pared with the theoretical results obtained in the full RPA-DF, the GLP, and the LP approaches. To allow for a sensible comparison we have set $\hbar\eta$ to 0.7 K, chosen to reproduce the experimental maximum value of $\hat{S}$. The figure shows a better agreement with experiment of the less involved LP and GLP approaches than of the full RPA-DF approach since the zero-soundlike dispersion displayed in the top right panel neither shows the slope nor the strength of the experimental data displayed in the top left panel. It is worthwhile seeing that within the GLP method, the low-energy branch still displays a ph bandlike shape because of the smallness of x_3.

To complete the analysis using the three theoretical approaches, the "ph band" at $T=0$, $P=12.7$ bars, and $x_3=5\%$ corresponding to $q=1.3$ Å^{-1} is represented in Fig. 9 and compared with the experimental results at $T=70$ mK.[16] The function $\hat{S}^{(3)}$ plotted in this figure is defined as

$$\hat{S}^{(3)} = \left[1 + \frac{\sigma_4^c(1-x_3)}{(\sigma_3^c+\sigma_3^i)x_3}\right]\hat{S}$$

so that if $S^{(4)}=S^{(x)}=0$ then $\hat{S}^{(3)}/\rho=S^{(3)}/\rho_3$. It is apparent how the negative $S^{(x)}$ contribution in the GLP approach diminishes the strength with respect to the LP ph band, resulting in a better agreement with experiment. This effect was qualitatively anticipated in Ref. 15.

We represent in Fig. 10 the results obtained in the GLP approximation for $P=10$ bars and $x_3=1\%$, 5%, 7%, and 9%. A "bite" (dampening) in the roton dispersion caused by its crossing of the ph band is clearly visible. We want to stress that within the RPA and the GLP approaches, this dampening is due to the coupling between both responses caused by the W_x term. Other dampening effects might contribute to wash out this effect. If their effect is qualitatively represented by the outcome of increasing $\hbar\eta$ from 0.1 to 0.7 K, it would clearly affect the appearance of the dampening, as can be appreciated by comparing the top right panel of Fig. 10 with the bottom left panel of Fig. 8, where the crossing hardly produces a shoulder in the phonon-roton branch.

Finally, we want to mention that at small energies and low-q values we have also found a collective excitation that does not show up in the LP approximation, indicating that the W_x ph potential alone does produce some collective behavior. As shown in Fig. 10, this peak is located outside the ph band and is Landau dampened when it gets into it. It remains an open question whether it is an artifact of the RPA-DF approach or not, as it is too low in energy to be detected by neutron scattering.[16]

IV. SUMMARY

We have studied the dynamic structure function of superfluid ^{3}He-^{4}He mixtures at zero temperature as a function of pressure and ^{3}He concentration within the RPA-DF framework, thus completing the description of the thermodynamics and elementary excitations of liquid-helium mixtures at $T=0$ within this phenomenological approach, that has the merit of providing the particle-hole interactions out of which one may obtain close-analytic expressions for the response functions, as well as for some sum rules of the dynamic structure function that may be used to determine average energies for the collective excitations.

The dispersion relation of the collective excitations presents a strong level repulsion between zero-soundlike and phonon-rotonlike excitations, whose gap increases as x_3 does. The analytic expressions for the average energies obtained from the sum rules compare well with the energies of the collective modes inferred from the total scattering function $\hat{S}(q,\omega)$ by inspection.

We have found that the cross term $S^{(x)}$ plays a non-negligible role in the appearance of the total scattering func-

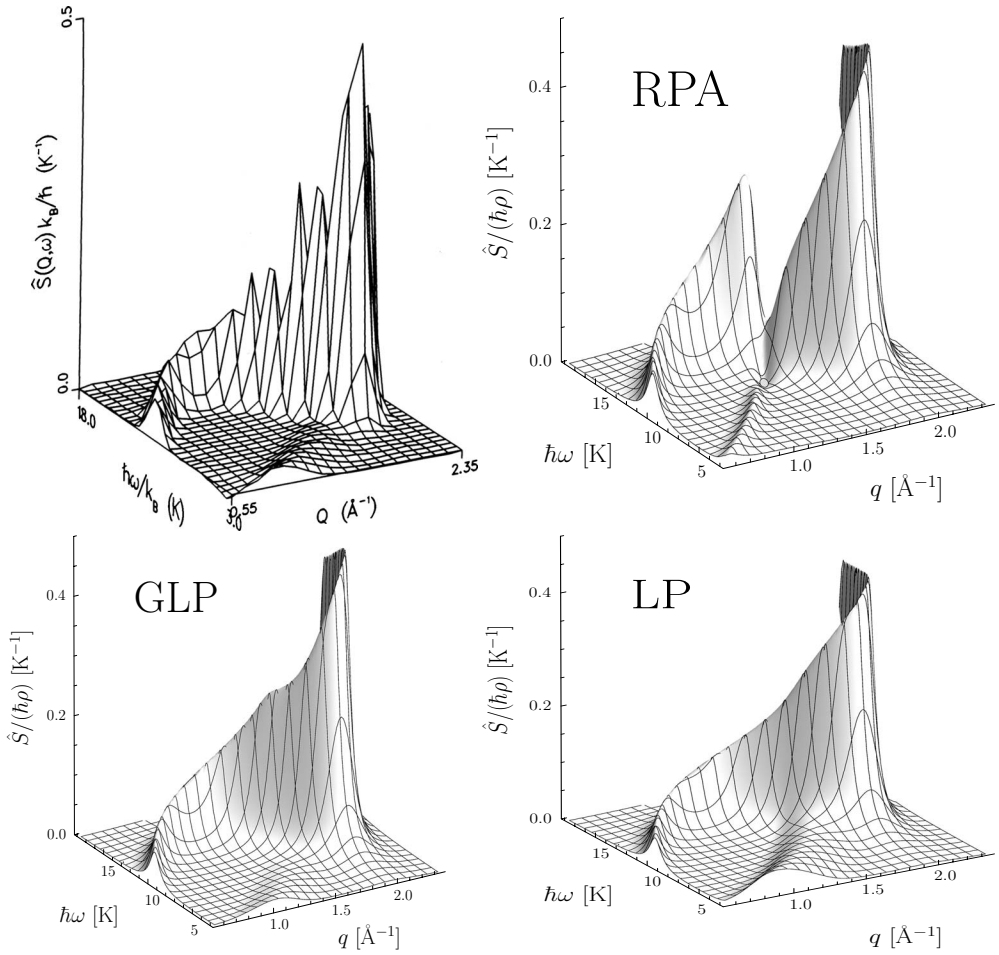

FIG. 8. Top left panel: experimental data by Fåk *et al.* (Ref. 16) at SVP for $T=70$ mK and $x_3=5\%$; the saw-tooth ridge of the phonon-roton excitation is an artifact of the plotting routine (Ref. 16). Top right panel: result of the full RPA-DF approach. Botton left panel: generalized Landau-Pomeranchuk result. Botton right panel: Landau-Pomeranchuk result. All the calculations have been carried out using $\hbar\eta=0.7$ K.

tion, although its q and ω dependence is so similar to that of $S^{(4)}$ and $S^{(3)}$ terms that its contribution may be difficult to disentangle. This term is also responsible for a strong hybridization of the collective modes.

The experimental results indicate that, contrarily to RPA results, no collective zero sound appears but instead a p-h band is clearly visible. We have checked that this disagreement remains when the full interactions $V_{ph}^{(3,3)}$ and $V_{ph}^{(3,4)}$ are employed instead of their Landau-type approximations, Eqs. (16) and (17). In fact, we have found that they both sensibly yield the same results. It is worth recalling that the microscopic Fermi hypernetted chain plus RPA calculations of Ref. 8 also predict the existence of a prominent collective zero sound. This indicates that the disagreement with experiment arises from the use of the RPA and not from a limitation inherent to DFT, and for that reason we have resorted to a generalized Landau-Pomeranchuk approach to obtain $\hat{S}(q,\omega)$. In this approach, the more intense ph interactions, namely, $V_{ph}^{(4,4)}$ and $V_{ph}^{(3,4)}$, are kept but $V_{ph}^{(3,3)}$ is artificially set to zero (the LP approximation also ignores the $V_{ph}^{(3,4)}$ term). Within this approximation, we have determined that the effect of keeping the $V_{ph}^{(3,4)}$ interaction appears as a dampening in the phonon-roton branch, which does not show up in the LP approximation, and as a collective peak at low energies and transferred momenta outside the range accessible by neutron-scattering experiments. This collective peak is washed out as it gets into the ph band. The main results obtained within the GLP approximation compare well with

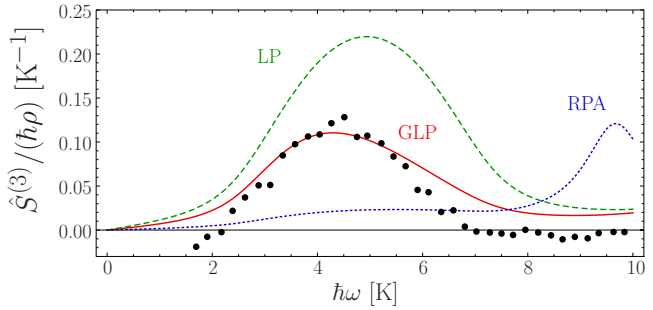

FIG. 9. (Color online) Particle-hole band at $P=12.7$ bars and $x_3=5\%$ corresponding to $q=1.3$ Å^{-1}. The experimental points (dots) are from Ref. 16. Solid line: generalized Landau-Pomeranchuk result. Dashed line: Landau-Pomeranchuk result. Dotted line: full RPA-DF result. All the calculations have been carried out using $\hbar\eta=0.7$ K.

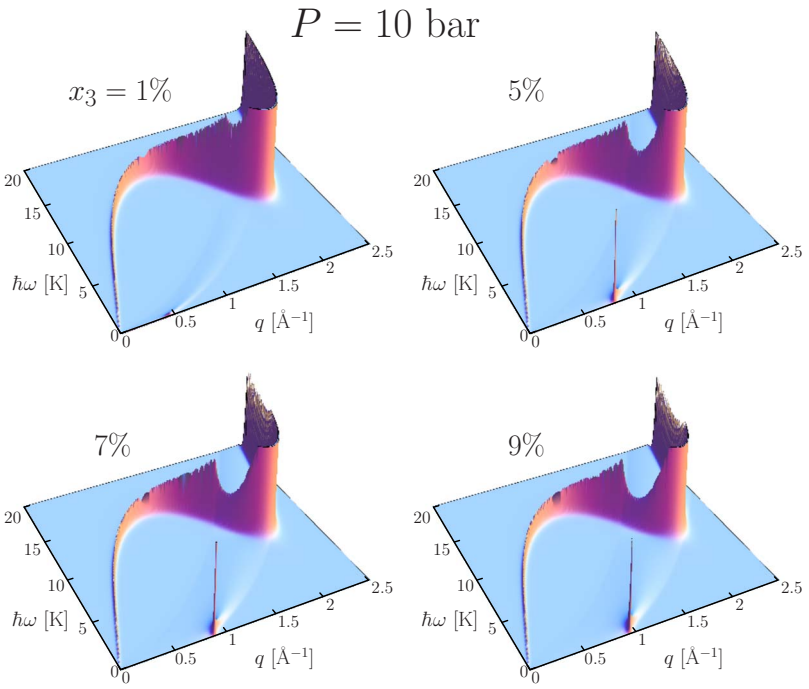

FIG. 10. (Color online) Same as Fig. 5 in the generalized Landau-Pomeranchuk approach. The dampening in the scattering function caused by the crossing of the ph band with the phonon-roton branch can be clearly seen.

the experiment, a hint on the correctness of the ph interactions derived from the DF approach, indicating on the other hand that the $V_{ph}^{(3,3)}$ interaction is quenched by a physical mechanism not included in the RPA description.

To go beyond RPA, more complicated intermediate states should be included in the calculation of the response function. In the so-called second RPA, introduced some years ago in Nuclear Physics (see, e.g., Ref. 41 and references therein), 2p-2h excitations are included together with the usual RPA 1p-1h ones. In the context of quantum fluids, the work of Ref. 42 has also shown the need of going beyond the RPA to describe dynamical properties of ^{3}He films.

ACKNOWLEDGMENTS

We acknowledge B. Fåk for providing us with the experimental results displayed in Fig. 8, as well as for useful comments. This work has been performed under Grants No. FIS2007-60133 and No. FIS2008-00421/FIS from DGI, Spain (FEDER), and Grant No. 2009SGR1289 from Generalitat de Catalunya. D.M. has been supported by the ME (Spain) FPU program, Grant No. AP2008-04343.

APPENDIX

In this appendix, we outline how can be shown that Eq. (26) still holds when the fermionic ph interaction is determined in the Landau approximation. We follow the procedure used in Refs. 43 and 44 for the case of more general ph interactions.

We start with the ph Green's function or retarded propagator $G^{(\alpha,\beta)}(q,\omega,\mathbf{k})$, where $\mathbf{k}$ is the momentum of the fermionic hole, which only appears if at least one of the indices α,β is equal to 3 (see Fig. 2). The response function $\chi^{(4,4)}(q,\omega)$ coincides with the corresponding Green's function, and for the others

$$\chi^{(3,\beta)}(q,\omega) = (1+\delta_{3,\beta})\int \frac{d^3k}{(2\pi)^3} G^{(3,\beta)}(q,\omega,\mathbf{k}), \quad \text{(A1)}$$

and analogously for $\chi^{(\alpha,3)}(q,\omega)$. To simplify the notation, we omit the q,ω dependence in the following but keep the hole momentum when present. We will also use the abridged notation

$$\langle G^{(\alpha,\beta)}\rangle = \int \frac{d^3k'}{(2\pi)^3} G^{(\alpha,\beta)}(\mathbf{k}'). \quad \text{(A2)}$$

For ph interactions given by Eqs. (15) and (16), the RPA equations can be cast into two sets of two coupled equations each. Let us first consider the coupling between $G^{(4,4)}$ and $G^{(3,4)}$,

$$G^{(4,4)} = G_0^{(4)} + G_0^{(4)} W_4 \langle G^{(4,4)}\rangle + G_0^{(4)} W_x \langle G^{(3,4)}\rangle,$$

$$G^{(3,4)}(\mathbf{k}) = G_0^{(3)}(\mathbf{k}) W_x \langle G^{(4,4)}\rangle + G_0^{(3)}(\mathbf{k}) f_0 \langle G^{(3,4)}\rangle + G_0^{(3)}(\mathbf{k}) f_1 \cos\theta \langle G^{(3,4)} \cos\theta'\rangle. \quad \text{(A3)}$$

Integrating the second equation over $\mathbf{k}$, one can see that the quantity $\langle G^{(3,4)}\rangle$ we are interested in is also coupled to $\langle G^{(3,4)} \cos\theta\rangle$. A further equation is obtained multiplying the second equation with $\cos\theta$ and integrating over $\mathbf{k}$. The new equation involves the following integrals related to the noninteracting fermionic propagator:

$$\gamma_i = \langle G_0^{(3)} (\cos\theta)^i\rangle \quad \text{(A4)}$$

for $i=0,1,2$. The integral for $i=0$ is the noninteracting response function $\chi_0^{(3)}$ apart from a factor of 2 due to the spin degeneracy. In the Landau limit (small k and finite ν), the other two integrals can be written as

$$\gamma_1 = \nu\gamma_0,$$

$$\gamma_2 = \nu^2 \gamma_0 - \frac{1}{6} N_0.$$

After some algebra, we get

$$\chi^{(4)} = \frac{\chi_0^{(4)}}{1 - W_4 \chi_0^{(4)} - \frac{1}{2} W_x \chi_0^{(4)} \frac{W_x \chi_0^{(3)}}{1 - \left(f_0 + \frac{f_1 \nu^2}{1 + F_1/3} \right) \chi_0^{(3)}}},$$

$$\chi^{(3,4)} = \frac{W_x \chi_0^{(4)} \chi_0^{(3)}}{(1 - W_4 \chi_0^{(4)}) \left[1 - \left(f_0 + \frac{f_1 \nu^2}{1 + F_1/3} \right) \chi_0^{(3)} \right] - \frac{1}{2} W_x^2 \chi_0^{(4)} \chi_0^{(3)}}. \quad \text{(A5)}$$

We consider now the coupling between the other two Green's functions $G^{(4,4)}$ and $G^{(3,4)}$,

$$G^{(4,3)}(\mathbf{k}) = G_0^{(4)} W_4 \langle G^{(4,3)} \rangle + G_0^{(4)} W_x \langle G^{(3,3)} \rangle,$$

$$G^{(3,3)}(\mathbf{k}) = G_0^{(3)}(\mathbf{k}) + G_0^{(3)}(\mathbf{k}) W_x \langle G^{(4,3)} \rangle + G_0^{(3)}(\mathbf{k}) f_0 \langle G^{(3,3)} \rangle + G_0^{(3)}(\mathbf{k}) f_1 \cos\theta \langle G^{(3,3)} \cos\theta' \rangle. \quad \text{(A6)}$$

Proceeding along the same lines as before, one finally gets

$$\chi^{(3)} = \frac{\chi_0^{(3)}}{1 - \left(f_0 + \frac{f_1 \nu^2}{1 + F_1/3} \right) \chi_0^{(3)} - \frac{1}{2} W_x \chi_0^{(3)} \frac{W_x \chi_0^{(4)}}{1 - W_4 \chi_0^{(4)}}},$$

$$\chi^{(4,3)} = \frac{W_x \chi_0^{(4)} \chi_0^{(3)}}{(1 - W_4 \chi_0^{(4)}) \left[1 - \left(f_0 + \frac{f_1 \nu^2}{1 + F_1/3} \right) \chi_0^{(3)} \right] - \frac{1}{2} W_x^2 \chi_0^{(4)} \chi_0^{(3)}}. \quad \text{(A7)}$$

Note that $\chi^{(3,4)} = \chi^{(4,3)}$ as expected. Thus, the monopolar and dipolar Landau interaction yields a (q, ω)-dependent ph interaction,

$$W_3(q, \omega) = f_0(q) + \frac{f_1 \nu^2}{1 + F_1/3}. \quad \text{(A8)}$$

From the above expressions, Eq. (26) is straightforwardly obtained.

[1] C. Ebner and D. O. Edwards, Phys. Rep. **2**, 77 (1971).
[2] M. Lücke and A. Szprynger, Phys. Rev. **26**, 1374 (1982).
[3] A. Szprynger and M. Lücke, Phys. Rev. **32**, 4442 (1985).
[4] R. De Bruyn Ouboter and C. N. Yang, Physica B **144**, 127 (1987).
[5] D. O. Edwards and M. S. Pettersen, J. Low Temp. Phys. **87**, 473 (1992).
[6] G. Chaudhry and J. G. Brisson, J. Low Temp. Phys. **155**, 235 (2009); **158**, 806 (2010).
[7] W. Hsu and D. Pines, J. Stat. Phys. **38**, 273 (1985).
[8] E. Krotscheck and M. Saarela, Phys. Rep. **232**, 1 (1993).
[9] G. Baym and C. Pethick, *Landau Fermi-Liquid Theory* (Wiley, New York, 1991).
[10] E. R. Dobbs, *Helium Three* (Oxford University Press, Oxford, 2000).
[11] D. O. Edwards, D. F. Brewer, P. Seligman, M. Skertic, and M. Yagub, Phys. Rev. Lett. **15**, 773 (1965).
[12] J. Bardeen, G. Baym, and D. Pines, Phys. Rev. **156**, 207 (1967).
[13] M. Weyrauch and A. Szprynger, Phys. Rev. B **51**, 12698 (1995).
[14] A. Fabrocini, L. Vichi, F. Mazzanti, and A. Polls, Phys. Rev. B **54**, 10035 (1996).
[15] J. Boronat, F. Dalfovo, F. Mazzanti, and A. Polls, Phys. Rev. B **48**, 7409 (1993).
[16] B. Fåk, K. Guckelsberger, M. Körfer, R. Scherm, and A. J. Dianoux, Phys. Rev. B **41**, 8732 (1990).
[17] M. Barranco, M. Pi, S. M. Gatica, E. S. Hernández, and J. Navarro, Phys. Rev. B **56**, 8997 (1997).
[18] F. Dalfovo, A. Lastri, L. Pricaupenko, S. Stringari, and J. Treiner, Phys. Rev. B **52**, 1193 (1995).
[19] S. Stringari and J. Treiner, Phys. Rev. B **36**, 8369 (1987); J. Chem. Phys. **87**, 5021 (1987).
[20] O. Bünermann, M. Dvorak, F. Stienkemeier, A. Hernando, R. Mayol, M. Pi, M. Barranco, and F. Ancilotto, Phys. Rev. B **79**, 214511 (2009).
[21] F. Ancilotto, M. Barranco, E. S. Hernández, and M. Pi, J. Low Temp. Phys. **157**, 174 (2009).
[22] D. Mateo, M. Pi, and M. Barranco, Phys. Rev. B **81**, 174510 (2010).
[23] M. Barranco, R. Guardiola, S. Hernández, R. Mayol, J. Navarro, and M. Pi, J. Low Temp. Phys. **142**, 1 (2006).
[24] E. Krotscheck and R. Zillich, J. Chem. Phys. **115**, 10161 (2001).
[25] M. Casas, F. Dalfovo, A. Lastri, Ll. Serra, and S. Stringari, Z. Phys. D **35**, 67 (1995).
[26] F. Garcias, Ll. Serra, M. Casas, and M. Barranco, J. Chem. Phys. **115**, 10154 (2001).
[27] F. Dalfovo and S. Stringari, Phys. Lett. A **112**, 171 (1985).
[28] H. C. Chocolacs, R. M. Mueller, J. R. Owers-Bradley, Ch. Buchal, M. Kubota, and F. Pobell, in *Low Temperature Physics LT17*, edited by U. Eckern, A. Schmid, W. Weber, and H. Wuhl (Elsevier, New York, 1984).
[29] Y. M. Engel, D. M. Brink, K. Goeke, S. J. Krieger, and D. Vautherin, Nucl. Phys. A **249**, 215 (1975).
[30] C. García-Recio, J. Navarro, N. Van Giai, and L. L. Salcedo, Ann. Phys. (N.Y.) **214**, 293 (1992).
[31] C. H. Aldrich and D. Pines, J. Low Temp. Phys. **25**, 677 (1976).
[32] C. H. Aldrich and D. Pines, J. Low Temp. Phys. **32**, 689 (1978).
[33] A. L. Fetter and J. D. Walecka, *Quantum Theory of Many-Particle Systems* (Mc-Graw Hill, Boston, 1971).
[34] O. Bohigas, A. M. Lane, and J. Martorell, Phys. Rep. **51**, 267 (1979).

[35] E. Lipparini and S. Stringari, Phys. Rep. **175**, 103 (1989).
[36] R. P. Feynman, Phys. Rev. **94**, 262 (1954).
[37] E. Lipparini, *Modern Many-Particle Physics: Atomic Gases, Quantum Dots and Quantum Fluids*, 2nd ed. (World Scientific, Singapore, 2008).
[38] H. R. Glyde and E. C. Svensson, in *Neutron Scattering*, Methods in Experimental Physics Vol. 23B, edited by D. L. Price and K. Sköld (Academic, New York, 1987), p. 303.
[39] J. Landau, J. T. Tough, N. R. Brubaker, and D. O. Edwards, Phys. Rev. Lett. **23**, 283 (1969).
[40] L. D. Landau and I. Pomeranchuk, Dokl. Akad. Nauk SSSR **59**, 669 (1948).
[41] D. Gambacurta, M. Grasso, and F. Catara, Phys. Rev. C **81**, 054312 (2010).
[42] H. M. Böhm, E. Krotscheck, M. Panholzer, H. Godfrin, H. J. Lauter, and M. Meschke, J. Low Temp. Phys. **158**, 194 (2010).
[43] J. Margueron, N. Van Giai, and J. Navarro, Phys. Rev. C **72**, 034311 (2005).
[44] J. Margueron, N. Van Giai, and J. Navarro, Phys. Rev. C **74**, 015805 (2006).